MATERIALS CHEMISTRY FRONTIERS

RESEARCH ARTICLE

View Article Online
View Journal | View Issue

Cite this: *Mater. Chem. Front.*, 2023, **7**, 3406

Underlayer engineering of grain strain toward efficient and stable tin perovskite solar cells†

Bo Li,[a] Zhen Li,[a] Danpeng Gao,[a] Xin Wu,[a] Xintong Li,[a] Chunlei Zhang,[a] Shuai Li,[a] Jianqiu Gong,[a] Dong Zhang,[a] Xiangfan Xie,[b] Shuang Xiao,*[b] Haipeng Lu,[c] Mingjie Li[d] and Zonglong Zhu*[ae]

Received 4th March 2023,
Accepted 11th May 2023

DOI: 10.1039/d3qm00236e

rsc.li/frontiers-materials

Lead-free tin perovskite solar cells (TPSCs) have gained prominence as a promising green photovoltaic technology. However, the rapid crystallization of tin perovskites leads to residual strain within the film, generating a large number of deep-level defects, which severely restrict the enhancement of power conversion efficiency (PCE) and lifetime of TPSCs. Here, we have developed an underlayer engineering strategy to release the residual compressive strain of tin perovskite films through the design of long-chain alkylamines as crystallization buffer molecules, which enhanced the photovoltaic performance and stability of TPSCs. Through tuning the backbone length of the alkylamines to modify the interface between the perovskite and hole transporting layer (HTL), octadecanammonium iodide (ODAI) was demonstrated to be the most effective to produce high-crystallinity and strain-free tin perovskite films. Moreover, the released residual strain can reduce the trap state density and suppress the nonradiative recombination in tin perovskite thin films. The resulting device with an ODAI underlayer achieved a champion PCE of 13.82% and a voltage of 0.818 V, respectively, maintained over 92% and 88% of initial PCE under continuous one sunlight illumination and 65° heating for 1000 hours.

Introduction

The striking optoelectronic properties, low-cost solution process and high reproducibility of perovskite solar cells (PSCs) have led to their tremendous development with efficiency approaching 26%.[1–6] However, the toxicity of lead in perovskite materials remains a challenge that must be addressed before commercialization.[7–9] Tin perovskites, a substitute for lead halide perovskites, perform better than other lead-free perovskite options owing to their ideal bandgap, high carrier mobility and favorable exciton binding energy.[10–18] However, tin PSCs (TPSCs) suffer from poor photovoltaic performance and air instability, owing to the easy generation of tin vacancies and divalent tin oxidation.[19] To address these challenges, a large number of strategies have been practiced in TPSCs, including the design of organic amine cations for dimensionality modulation, the application of antioxidants, the introduction of reducing atmospheres and the improvement of interfacial properties.[20–23] As a result of these accomplishments, TPSC has grown rapidly in recent years, and its efficiency has approached 15%.[24]

Rapid crystallization is another serious impediment for tin perovskites due to the unpredictable morphology and constrained grain size, which severely affects the performance and stability of TPSCs.[25] On one hand, the small grains generated by fast crystallization are accompanied by multiple grain boundaries, and the accumulating imperfections at the grain boundaries are harmful to the carrier generation and transfer.[26] On the other hand, the non-uniform grain size increases the perovskite interaction with water and oxygen, which influences the stability of TPSC.[27] Although considerable efforts have been devoted to the regulation of crystallization of tin perovskite films through solvent-, additive- and dimensional-engineering, the residual strain caused by the fast crystallization of the tin perovskite, as well as its impact on TPSC performance remain poorly understood.[28–34] Residual strain in perovskite films can significantly affect the photovoltaic performance by increasing the concentration of trap states, reducing carrier mobility, and leading to more non-radiative recombination.[35–39] Lattice strain can also destabilize the perovskite crystal structure, which is

[a] *Department of Chemistry, City University of Hong Kong, Kowloon, Hong Kong SAR, China. E-mail: zonglzhu@cityu.edu.hk*
[b] *Shenzhen Key Laboratory of Ultraintense Laser and Advanced Material Technology, Center for Advanced Material Diagnostic Technology, and College of Engineering Physics, Shenzhen Technology University, Shenzhen 518118, P. R. China. E-mail: shuangxiao@sztu.edu.cn*
[c] *Department of Chemistry, The Hong Kong University of Science and Technology, Kowloon, Hong Kong SAR, China*
[d] *Department of Applied Physics, The Hong Kong Polytechnic University, Hong Kong SAR, China*
[e] *City University of Hong Kong Shenzhen Research Institute, Shenzhen, Guangdong 518057, China*

† Electronic supplementary information (ESI) available. See DOI: https://doi.org/10.1039/d3qm00236e

associated with humidity, heat and light sensitivity.[40] Therefore, it is critical to understand strain formation in tin perovskites and rational molecular design to eliminate residual strain for improving both the efficiency and stability of TPSCs.

Previous studies have shown that the long-chain nature of organic molecules facilitates the formation of networks at grain boundaries, which can significantly optimize the quality and morphology of perovskite films.[41,42] In general, the chain length of amine molecules has three main influences on the perovskite films. First, alkylamine molecules can affect the grain size of perovskite films through anchoring on colloidal perovskite cores *via* amino groups. Stronger van der Waals forces of long-chain ligands can lead to more crystal growth inhibition.[43] Second, long-chain alkylamines can modulate the orientation of perovskite crystals, and the strong van der Waals force between the anchored long-chain alkylamines can enhance the binding between adjacent grains and promote the growth of perovskites in a specific direction.[44] Third, the chain length determines the distribution and position of the alkylamines, and long-chain alkylamines usually exhibit better defect passivation effects than short-chain ones due to the spontaneous repulsion through van der Waals forces and the steric hindrance induced by the large molecule size.[45]

In this work, an underlayer engineering strategy was developed through introducing long chain alkylamines as crystallization buffer molecules to modify the interface between the tin perovskite and hole transport layer (HTL) in inverted planar TPSCs. The tin perovskite films modulated through octadecanammonium iodide (ODAI) achieved the release of residual compressive strain and high crystallinity, which leads to reduced defect densities and suppressed non-radiative recombination. The optimal TPSCs with ODAI underlayers reached a PCE of 13.82% and a voltage of 0.818 V, respectively, and maintained over 92% and 88% of their initial efficiency after continuously illuminating and heating for 1000 hours. Our work reveals the residual compressive strain in tin perovskite films, providing guidance for improving the photovoltaic performance and stability of TPSCs from the perspective of buried interfacial strain regulation.

Results and discussion

The device structure of TPSC is shown in Fig. 1a, where the composition of the perovskite is $FA_{0.98}EDA_{0.01}SnI_3$, and C60 and poly(3,4-ethylenedioxythiophene) polystyrene sulfonate (PEDOT:PSS) are used as the electron transport layer (ETL) and HTL, respectively. Three long-chain alkylamines with different carbon backbone lengths (n) were used as an underlayer between the perovskite and HTL in inverted planar TPSCs, including octylammonium iodide (OAI), dodecylammonium iodide (DDAI) and octadecanammonium iodide (ODAI) as shown in Fig. 1b. The interactions between the perovskite and alkylamines were first studied though X-ray photoelectron spectroscopy (XPS). We directly deposited alkylamine molecules on the surface of the perovskite film and annealed them to mimic the real bottom interface molecular interactions.

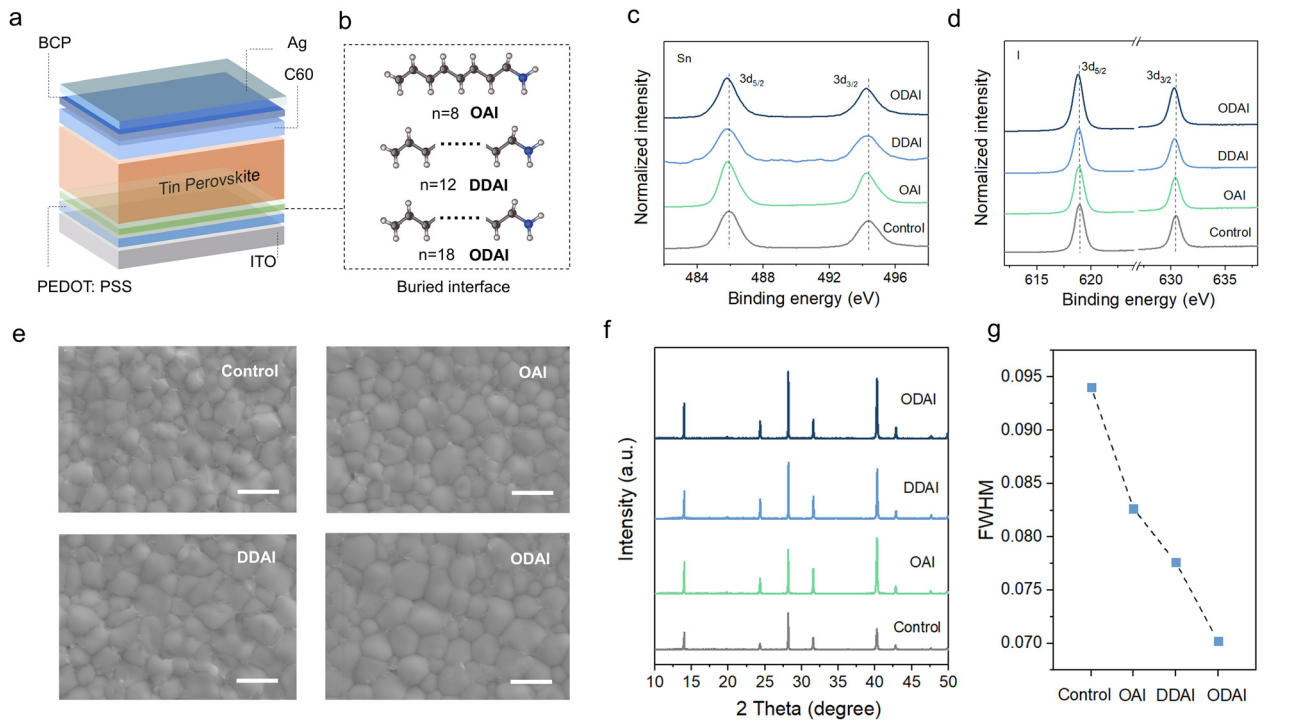

Fig. 1 (a) Schematic diagram of the device structure of TPSCs. (b) Three long-chain alkylamines as the buried interlayer, *i.e.* OAI, DDAI and ODAI. (c) and (d) XPS spectra of Sn and I elements for the pristine perovskite and alkylamine treated perovskite. (e) SEM images of the tin perovskite films with and without the alkylamine interlayer. The scale bar is 500 nm. (f) XRD spectra and (g) FWHM of the (001) crystal plane of the tin perovskite films with and without the alkylamine interlayer.

The binding energies of the Sn 3d and I 3d core levels of the perovskite films with alkyl ammonium all slightly decrease in comparison to the control ones, as seen in Fig. 1c and d. The reduction of electron binding energy at the core level indicates the formation of a strong interaction between the perovskite and alkylamine interface, and is also indicative of reduction in the oxidation state of Sn, which in turn leads to the reduction of the oxidation state of I.[46,47]

The morphologies of the tin perovskite film are shown in the scanning electron microscopy (SEM) images in Fig. 1e. The pristine perovskite film exhibits non-uniform crystal grain distribution with size ranging from 50 nm to 500 nm. After introducing long-chain alkylamines, the perovskite crystal grain size increases, accompanied by improved uniformity. The perovskite films deposited on the ODAI underlayer show the largest grain size and optimal crystal grain homogeneity. In addition to the film morphology, we also estimate the crystallization of the tin perovskite films through X-ray diffraction (XRD). The tin perovskite films prepared using the long chain alkylamines exhibit significantly enhanced diffraction intensity compared to the control film, and the film on the ODAI underlayer shows the highest peak intensity, which is consistent with the morphology evolution shown in Fig. 1e. Moreover, the full width at half maximum (FWHM) of the (001) plane in Fig. 1g shows a gradual decline trend with the increase of the carbon backbone length, which further proves that introducing and increasing the length of the alkyl chain can improve the crystallinity of tin perovskite thin films.[48] The optical properties of tin perovskite films shown in the UV-vis absorption spectra (Fig. S1, ESI†) do not display obvious difference with the addition of the alkylamine underlayer.

To further investigate the residual strain in perovskite films, we conducted grazing incidence X-ray diffraction (GIXRD) measurements that utilize a small incident angle X-ray beam to limit penetration into the perovskite films. The GIXRD measurements were conducted by changing the incidence

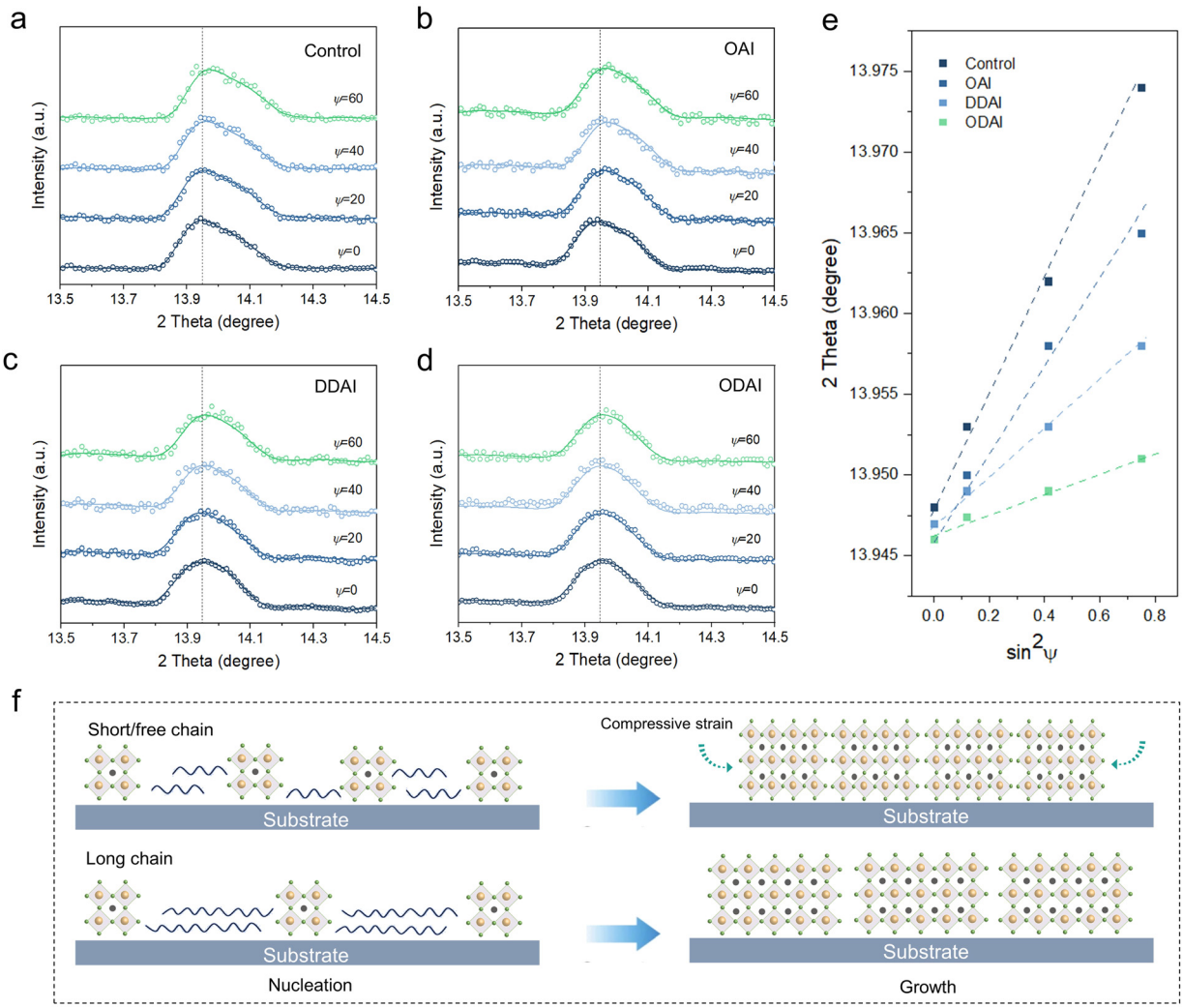

Fig. 2 Normalized GIXRD patterns of (a) the control perovskite film and the perovskite films coated on (b) OAI, (c) DDAI and (d) ODAI by varying the incidence angle from 0° to 60°. (e) Shift of the peak position (2θ) as a function of $\sin^2\psi$ for different perovskite films based on the (001) crystal plane. (f) Schematic illustrations of the nucleation and growth of perovskite thin films assisted by different underlayers and corresponding strain evolution.

angle φ over a fixed 2θ, which corresponds to the in-plane residual strain.[49] As φ = 0, the out-of-plane lattice distance completely determines the X-ray beam path, disregarding the in-plane information. When φ increases, the in-plane distance contributes more to the X-ray beam path, causing the peak of tensile strain along the in-plane direction to lower 2θ, while the peak of compressive strain to higher 2θ.[49] The (001) diffraction peak was selected for strain studies, and the fitted values are shown in Fig. S2 (ESI†). The GIXRD plots of tin perovskite films with and without alkylamines are shown in Fig. 2a to d, with φ increasing from 0 to 60 degrees. The tin perovskite film deposited on PEDOT:PSS shows a peak shift to higher 2θ with the increase of φ, demonstrating that the perovskite crystals are under compressive strain. When introducing alkylamine underlayers, the tendency of the peak shift decreases as shown in Fig. 2e, and a negligible shift is observed when introducing ODAI. The decreasing slope in Fig. 2e indicates that the compressive strain has been released with increasing carbon backbone length.

Fig. 2f displays a possible nucleation and crystallization mechanism of tin perovskite thin films with and without alkylamine interlayers. In the case of pristine or short chain alkylamines, the tin perovskite can produce more nucleation sites and faster crystallization speed, resulting in the formation of mutual extrusion and compression strain between crystal grains. In contrast, long chain alkylamines can be anchored on the colloidal perovskite core through amino groups during the wet film and nucleation stages. Due to the stronger van der Waals force and the steric hindrance caused by the larger molecule size, long chain amine molecules can act as crystallization buffer molecules to reduce the amount of perovskite nucleation and slow down the perovskite crystallization rate, which are beneficial to strain release for the formed perovskite films. The cross-sectional SEM images of the perovskite films in Fig. S3 (ESI†) further confirm this speculation, in which the pristine perovskite film exhibits disordered grain size and distribution throughout the film, and in contrast, the film deposited on the ODAI underlayer exhibits relatively orderly and uniform grain distribution.

For determining the residual strain in perovskite films, we further conducted steady-state photoluminescence (PL) and time-resolved photoluminescence (TRPL) characterization on

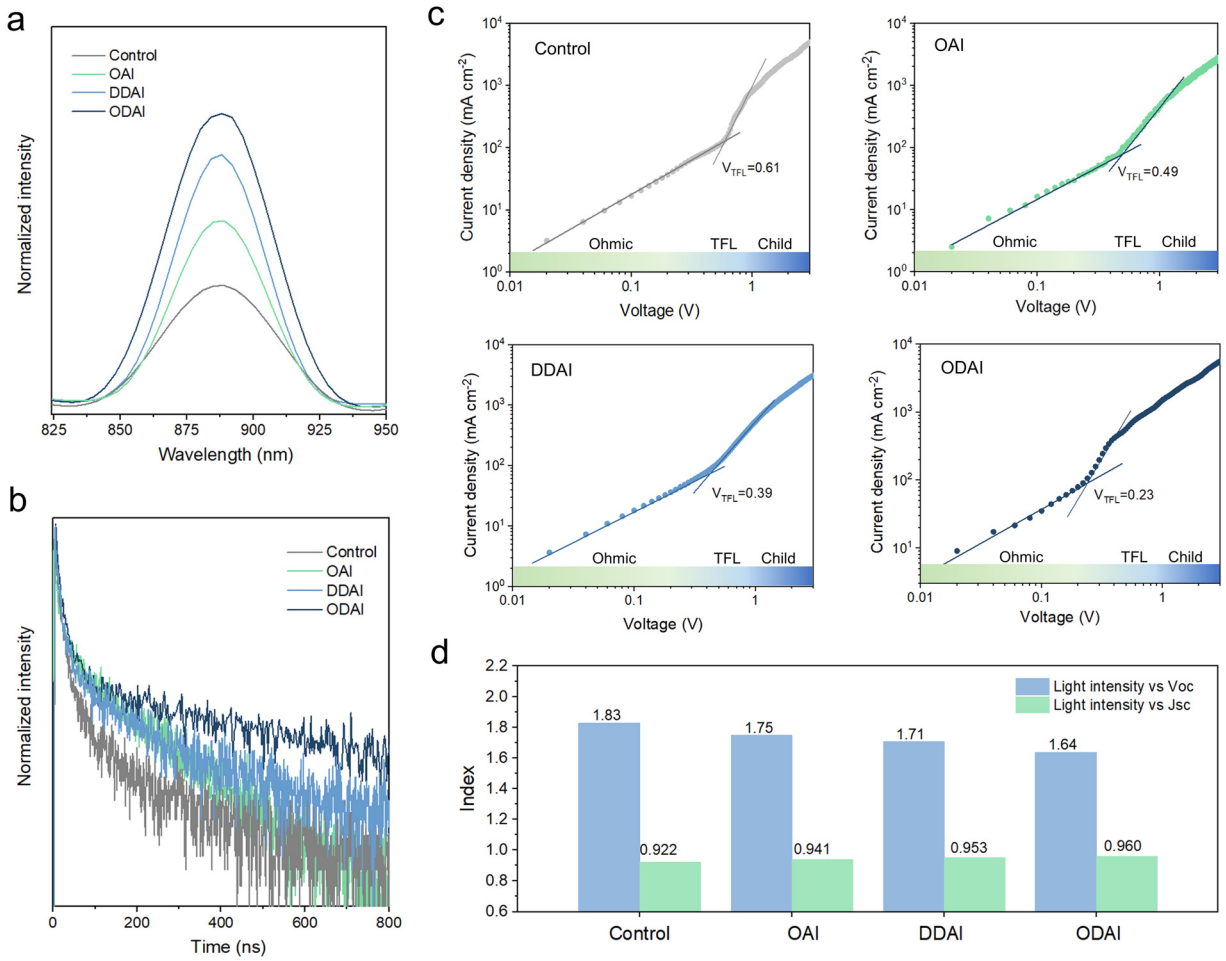

Fig. 3 (a) PL and (b) TRPL spectra of the control perovskite film and the perovskite films coated on OAI, DDAI and ODAI underlayers. (c) SCLC curves of control and modified perovskites with OAI, DDAI and ODAI underlayers. (d) Statistics of V_{OC} and J_{SC} *vs.* light intensity of the control and alkylamine modified perovskites.

tin perovskite films deposited on glass as shown in Fig. 3a and b. After introducing the alkylamine underlayer and increasing the backbone length, the tin perovskite films show a higher PL intensity than the pristine films (Fig. 3a). Furthermore, the carrier lifetime obtained by fitting the TRPL spectra increased from 180.4 ns for the control film to 416.3 ns for the ODAI treated film. These results suggest that the trap-assisted non-radiative recombination in tin perovskite films is suppressed after the introduction of alkylamine interlayers, and the tin perovskite film exhibits a minimal recombination loss on incorporating ODAI.

To quantify the defect density of states, we conducted space-charge-limited-current (SCLC) measurements on tin perovskites in the presence and absence of alkylamines. The equivalent current–voltage curves for a hole-only device are presented in Fig. 3c. The defect density of states (N_t) can be derived based on the equation $V_{TFL} = eN_tL^2/2\varepsilon\varepsilon_0$ (V_{TFL} is the trap-filling voltage, L is the perovskite film thickness, and ε_0 and ε represent the vacuum permittivity and relative dielectric constant).[50] The pristine perovskite film deposited on PEDOT:PSS shows a V_{TFL} value of 0.61 V. After incorporating alkylamines, the V_{TFL} value decreases to 0.49 V for OAI, 0.39 V for DDAI and 0.23 V for ODAI. The reduced trap density can be attributed to the release of residual compressive strains, which in turn reduces the potential formation of defects such as voids and dislocations.

Additionally, the light intensity dependent voltage–current curves are shown in Fig. S4 and S5 (ESI†). Fig. 3 shows the key parameter values extracted from the light intensity dependent current–voltage curves. Through linearly fitting the open-circuit voltages *versus* the logarithm of light intensity, the slopes for the control, OAI, ODAI and DDAI underlayer treated devices are $1.83K_BT/q$, $1.75K_BT/q$, $1.71K_BT/q$ and $1.64K_BT/q$, respectively (where K_B is the Boltzmann constant, and T and q represent absolute temperature and elementary charge). Ideally, the

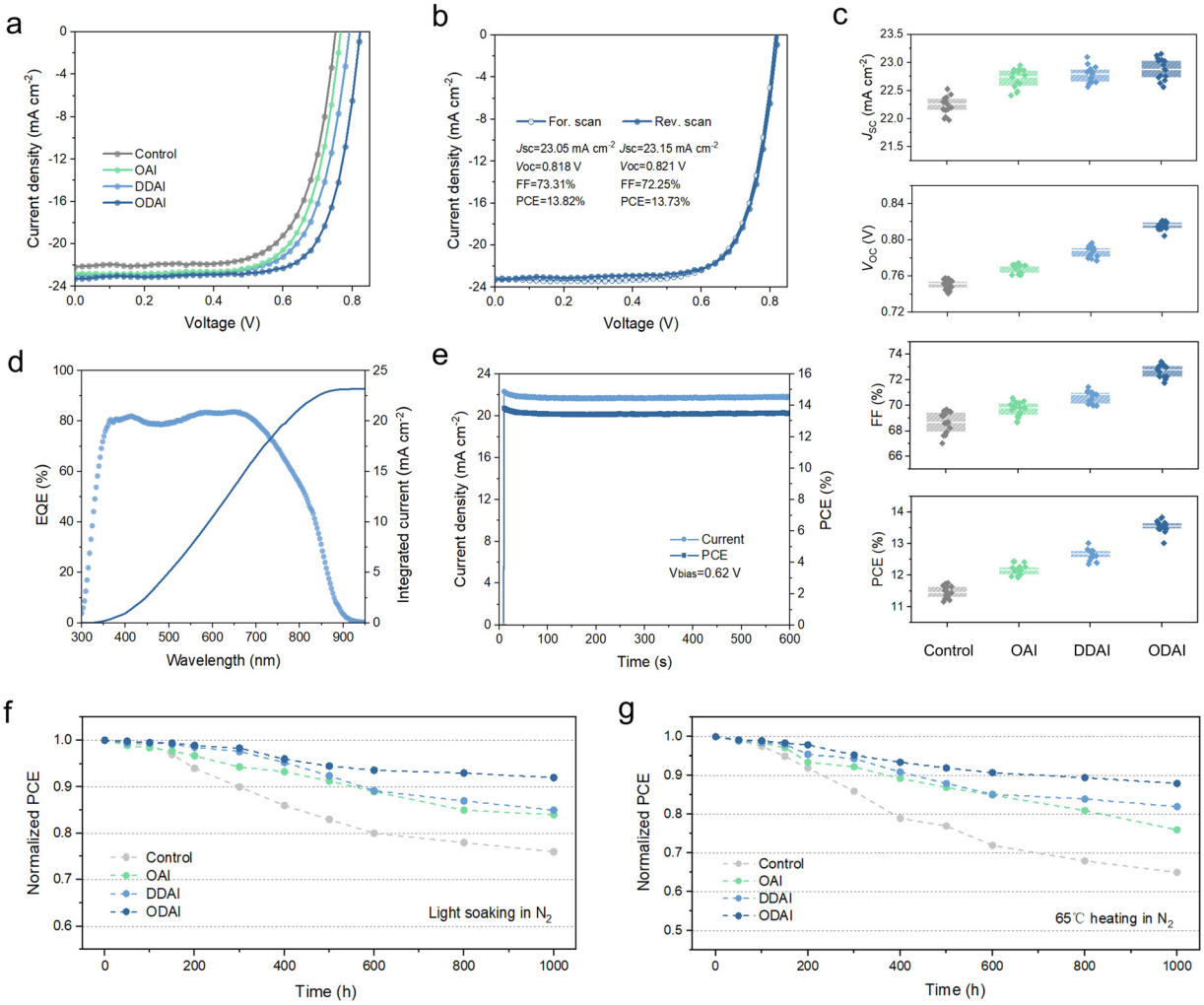

Fig. 4 (a) J–V curves of the champion TPSCs without and with different alkylamines. (b) J–V curve of the champion TPSCs with the ODAI interlayer under forward and reverse scans. (c) Photovoltaic parameter statistics for TPSCs without and with different alkylamines. (d) EQE plots and integrated current of the best performing TPSC. (e) Stabilized current and efficiency of the best performing TPSC under continuous illumination. (f) Light stability measurements of the unencapsulated devices at room temperature in N_2 under continuous AM 1.5 G sunlight illumination. (g) Heat stability measurements of the unencapsulated devices in N_2 under 65 °C heating.

ideality factor n value in the slope nK_BT/q is 1 in the absence of trap-assisted recombination, whereas any deviation from the ideal value indicates the presence of trap-assisted recombination. The n value decreased from 1.83 in the control device to 1.64 in the device with the ODAI underlayer, suggesting that trap-assisted nonradiative recombination is hindered.[51] Similarly, the power-law dependence of current density on the light intensity can be represented by $J_{SC} \propto (P_{light})^{\alpha}$ ($\alpha \leq 1$). The slope of the light intensity dependency of J_{SC} for the ODAI modified TPSC is 0.960, higher than 0.922 for the control one, which further demonstrates the inhibited nonradiative recombination of tin perovskite films due to the release of residual strain by introducing long-chain alkylamines.[52]

The photovoltaic performance of the TPSCs with and without the alkylamine underlayer was investigated through fabricating an inverted device with a structure of indium tin oxide (ITO)/poly(3,4-ethylenedioxythiophene):poly(styrene sulfonate) (PEDOT:PSS)/alkylamines/perovskite/C_{60}/2,9-dimethyl-4,7-diphenyl-1,10 phenanthroline (BCP)/silver (Ag). The photovoltaic performances of all TPSCs with different concentrations of alkylamines were studied and are shown in Fig. S6 to S8 (ESI†). By horizontal comparison according to the different concentrations of each underlayer, the increase of concentration from 0.5 mg mL^{-1} to 1.5 mg mL^{-1} leads to an ascending and then descending PCE evolution, where the devices with 1.0 mg mL^{-1} alkylamines exhibit highest efficiency. By longitudinally comparing different underlayers under the same concentration conditions, increasing the length of the alkyl chains results in gradually enhanced photovoltaic performance, and ODAI-modified TPSCs all show the best efficiency for all concentrations.

The photovoltaic performances of the best-performing TPSCs are determined from the current–voltage (J–V) curves in Fig. 4a. The pristine TPSC exhibits a champion PCE of 11.74%, with an open-circuit voltage (V_{OC}) of 0.757 V, a short-circuit current density (J_{SC}) of 22.26 mA cm^{-2} and a fill factor (FF) of 69.66%. After introducing OAI and DDAI, the V_{OC} shows a significant increase to 0.772 V and 0.792 V, which leads to the enhanced PCE of 12.42% and 12.99%, respectively. The incorporation of ODAI results in an efficiency of 13.82%, with a V_{OC} of 0.818 V, a J_{SC} of 23.05 mA cm^{-2} and an FF of 73.3%. As a comparison, we also investigated the photovoltaic performance of TPSCs prepared with tridodecylmethylammonium iodide (TDAI) with longer alkyl chains as shown in Fig. S9 (ESI†). In contrast, further increasing the alkyl chain length to TDAI causes an obvious decrease in the photovoltaic performance, which can be attributed to the hindered carrier transport and extraction at the buried interface, as confirmed by the PL quenching experiments in Fig. S10 (ESI†). These results further confirm that the TPSCs modified with the ODAI underlayer show the best photovoltaic performance, derived from the released lattice strain, and the resulting reduction of defect concentration and non-radiative recombination.

Fig. 4b shows the J–V curves of the best-performance TPSCs with ODAI as the underlayer with forward and reverse scanning. The device obtains PCEs of 13.82% and 13.73% under forward scanning and reverse scanning respectively, showing a considerable reduced hysteresis compared to other TPSCs in Fig. S11 to S13 (ESI†). Furthermore, Fig. 4c shows that each solar cell parameter is improved compared to those of the control device with the addition of alkylamine, and V_{OC} and FF show gradual increases with the increase of the carbon backbone length, which finally leads to the champion performance for the ODAI based device. The integrated J_{SC} obtained from the external quantum efficiency (EQE) in Fig. 4d exhibits a small deviation from the value in the J–V measurements. In addition, a stabilized photocurrent of 21.72 mA cm^{-2} and the corresponding stabilized PCE of 13.46% are achieved for the best-performing device at the maximum power point (MPP) (Fig. 4e).

For studying the influence of alkylamine underlayers on the stability of TPSC, we recorded the PCE evolution of the unencapsulated devices stored in an N_2 atmosphere under continuous light conditions (AM 1.5 G simulated sunlight) and continuous 65 °C heating, respectively, as shown in Fig. 4f and g. For the light stability test, we observed that all devices exhibit stability for the initial 150 hours (Fig. 4f). As the aging increases to 300 hours, the control device shows a rapid efficiency decay to around 90%, while the device with the ODAI underlayer still maintained over 98% of initial efficiency. After 1000 hours of illumination, the TPSCs with the ODAI underlayer retained more than 92% of initial PCE, which demonstrates a significant increase in the light stability, as compared to the over 20% efficiency degradation for the control device. In addition, we also tested the thermal stability of the device by heating the unencapsulated device at 65 °C in an N_2 environment. For the thermal stability shown in Fig. 4g, the ODAI-treated TPSCs maintained around 90% of the initial PCE after 800 h, while the value for the control device declined to below 70%. The improvement in light and heat stability might be attributed to the release of residual strain and improved crystallinity in the film to effectively overcome crystal lattice instability under heating and reduce the defect generation during illumination.

Conclusion

In summary, we have demonstrated the existence of compressive strains in tin perovskite films, and developed an underlayer engineering strategy to achieve the release of residual strain in tin perovskite films by introducing OAI, DDAI and ODAI. The results reveal that long chain alkylamine can modulate perovskite crystallization and growth, leading to release of residual compressive strain, which reduces the defect density, increases the carrier lifetime, and suppresses the non-radiative recombination loss in the tin perovskite films. The TPSCs with an ODAI underlayer achieved a highest power conversion efficiency of 13.82%, and maintained over 92% and 88% of initial PCE under continuous one-sun illumination and 65 °C heating for 1000 hours. This work reveals the strain state in tin perovskites and provides guidance for improving the photovoltaic performance and stability of TPSCs from the perspective of buried interfacial strain regulation.

Conflicts of interest

The authors declare no competing interests.

Acknowledgements

The work was supported by the Innovation and Technology Fund (GHP/100/20SZ, GHP/102/20GD, MRP/040/21X), the GRF grant (11306521) from the Research Grants Council of Hong Kong, the Green Tech Fund (GTF202020164), the Science Technology and Innovation Committee of Shenzhen Municipality (SGDX20210823104002015, JCYJ20220818101018038, 2022378670), the National Natural Science Foundation of China (2221101051, 21905006), and the Guangdong Provincial Science and Technology Plan (2021A0505110003).

References

1 A. Kojima, K. Teshima, Y. Shirai and T. Miyasaka, Organometal halide perovskites as visible-light sensitizers for photovoltaic cells, *J. Am. Chem. Soc.*, 2019, **131**, 6050–6051.
2 S. Bai, P. Da, C. Li, Z. Wang, Z. Yuan, F. Fu, M. Kawecki, X. Liu, N. Sakai, J. T. Wang, S. Huettner, S. Buecheler, M. Fahlman, F. Gao and G. J. Snaith, Planar perovskite solar cells with long-term stability using ionic liquid additives, *Nature*, 2019, **571**, 245–250.
3 N. Li, X. Niu, L. Li, H. Wang, Z. Huang, Y. Zhang, Y. Chen, X. Zhang, C. Zhu, H. Zai, Y. Bai, S. Ma, H. Liu, X. Liu, Z. Guo, G. Liu, R. Fan, H. Chen, J. Wang, Y. Lun, X. Wang, J. Hong, H. Xie, D. S. Jakob, X. G. Xu, Q. Chen and H. Zhou, Liquid medium annealing for fabricating durable perovskite solar cells with improved reproducibility, *Science*, 2021, **373**, 561–567.
4 Z. Dai, S. K. Yadavalli, M. Chen, A. Abbaspourtamijani, Y. Qi and N. P. Padture, Interfacial toughening with self-assembled monolayers enhances perovskite solar cell reliability, *Science*, 2021, **372**, 618–622.
5 S. Chen, X. Dai, S. Xu, H. Jiao, L. Zhao and J. Huang, Stabilizing perovskite-substrate interfaces for high-performance perovskite modules, *Science*, 2021, **373**, 902–907.
6 Z. Li, B. Li, X. Wu, S. A. Sheppard, S. Zhang, D. Gao, N. J. Long and Z. Zhu, Organometallic-functionalized interfaces for highly efficient inverted perovskite solar cells, *Science*, 2022, **376**, 416–420.
7 J. Cao and F. Yan, Recent progress in tin-based perovskite solar cells, *Energy Environ. Sci.*, 2021, **14**, 1286–1325.
8 Z. Li, X. Wu, B. Li, S. Zhang, D. Gao, Y. Liu, X. Li, N. Zhang, X. Hu, C. Zhi, A. K.-Y. Jen and Z. Zhu, Sulfonated graphene aerogels enable safe-to-use flexible perovskite solar modules, *Adv. Energy Mater.*, 2021, **12**, 2103236.
9 Z. Li, X. Wu, S. Wu, D. Gao, H. Dong, F. Huang, X. Hu, A. K.-Y. Jen and Z. Zhu, An effective and economical encapsulation method for trapping lead leakage in rigid and flexible perovskite photovoltaics, *Nano Energy*, 2022, **93**, 106853.
10 F. Hao, C. C. Stoumpos, D. H. Cao, R. P. H. Chang and M. G. Kanatzidis, Lead-free solid-state organic–inorganic halide perovskite solar cells, *Nat. Photonics*, 2014, **8**, 489–494.
11 G. Li, Z. Su, M. Li, F. Yang, M. H. Aldamasy, J. Pascual, F. Yang, H. Liu, W. Zuo, D. D. Girolamo, Z. Iqbal, G. Nasti, A. Dallmann, X. Gao, Z. Wang, M. Saliba and A. Abate, Ionic liquid stabilizing high-efficiency tin halide perovskite solar cells, *Adv. Energy Mater.*, 2021, **11**, 2101539.
12 B. Li, H. Di, B. Chang, R. Yin, L. Fu, Y. Zhang and L. Yin, Efficient Passivation Strategy on Sn Related Defects for High Performance All-Inorganic $CsSnI_3$ Perovskite Solar Cells, *Adv. Funct. Mater.*, 2021, **31**, 2007447.
13 M. Hu, R. Nie, H. Kim, J. Wu, S. Chen, B.-W. Park, G. Kim, H.-W. Kwon and S. I. Seok, Regulating the surface passivation and residual strain in pure tin perovskite films, *ACS Energy Lett.*, 2021, **6**, 3555–3562.
14 C. Wang, Y. Zhang, F. Gu, Z. Zhao, H. Li, H. Jiang, Z. Bian and Z. Liu, Illumination durability and high-efficiency Sn-based perovskite solar cell under coordinated control of phenylhydrazine and halogen ions, *Matter*, 2021, **4**, 709–721.
15 X. Meng, Y. Wang, J. Lin, X. Liu, X. He, J. Barbaud, T. Wu, T. Noda, X. Yang and L. Han, Surface-controlled oriented growth of $FASnI_3$ crystals for efficient lead-free perovskite solar cells, *Joule*, 2020, **4**, 902–912.
16 B. Chang, B. Li, Z. Wang, H. Li, L. Wang, L. Pan, Z. Li and L. Yin, Efficient Bulk Defect Suppression Strategy in $FASnI_3$ Perovskite for Photovoltaic Performance Enhancement, *Adv. Funct. Mater.*, 2022, **32**, 2107710.
17 X. Jiang, Z. Zang, Y. Zhou, H. Li, Q. Wei and Z. Ning, Tin halide perovskite solar cells: an emerging thin-film photovoltaic technology, *Acc. Mater. Res.*, 2021, **2**(4), 210–219.
18 B. Li, X. Wu, S. Zhang, Z. Li, D. Gao, X. Chen, S. Xiao, C.-C. Chueh, A. K.-Y. Jen and Z. Zhu, Efficient and stable $Cs_2AgBiBr_6$ double perovskite solar cells through in-situ surface modulation, *Chem. Eng. J.*, 2022, **446**, 137144.
19 R. Nishikubo, N. Ishida, Y. Katsuki, A. Wakamiya and A. Saeki, Minute-Scale Degradation and Shift of Valence-Band Maxima of $(CH_3NH_3)SnI_3$ and $HC(NH_2)_2SnI_3$ Perovskites upon Air Exposure, *J. Phys. Chem. C*, 2017, **121**, 19650–19656.
20 W. Ke, C. C. Stoumpos, I. Spanopoulos, L. Mao, M. Chen, M. R. Wasielewski and M. G. Kanatzidis, Efficient Lead-Free Solar Cells Based on Hollow {en}$MASnI_3$ Perovskites, *J. Am. Chem. Soc.*, 2017, **139**, 14800–14806.
21 B. Li, X. Wu, H. Zhang, S. Zhang, Z. Li, D. Gao, C. Zhang, M. Chen, S. Xiao, A. K.-Y. Jen, S. Yang and Z. Zhu, Efficient and Stable Tin Perovskite Solar Cells by Pyridine-Functionalized Fullerene with Reduced Interfacial Energy Loss, *Adv. Funct. Mater.*, 2022, **32**, 2205870.
22 Q. Tai, X. Guo, G. Tang, P. You, T. W. Ng, D. Shen, J. Cao, C. K. Liu, N. Wang, Y. Zhu, C. S. Lee and F. Yan, Antioxidant Grain Passivation for Air-Stable Tin-Based Perovskite Solar Cells., *Angew. Chem., Int. Ed.*, 2019, **58**, 806–810.
23 T. B. Song, T. Yokoyama, C. C. Stoumpos, J. Logsdon, D. H. Cao, M. R. Wasielewski, S. Aramaki and M. G. Kanatzidis, Importance of Reducing Vapor Atmosphere in the Fabrication of Tin-Based Perovskite Solar Cells, *J. Am. Chem. Soc.*, 2017, **139**, 836–842.
24 B.-B. Yu, Z. Chen, Y. Zhu, Y. Wang, B. Han, G. Chen, X. Zhang, Z. Du and Z. He, Heterogeneous 2D/3D tin-

halides perovskite solar cells with certified conversion efficiency breaking 14%, *Adv. Mater.*, 2021, **33**, 2102055.
25 B. Li, B. Chang, L. Pan, Z. Li, L. Fu, Z. He and L. Yin, Tin-based defects and passivation strategies in tin-related perovskite solar cells, *ACS Energy Lett.*, 2020, **5**(12), 3752–3772.
26 T. S. Sherkar, C. Momblona, L. Gil-Escrig, J. Avila, M. Sessolo, H. J. Bolink and L. J. A. Koster, Recombination in Perovskite Solar Cells: Significance of Grain Boundaries, Interface Traps, and Defect Ions, *ACS Energy Lett.*, 2017, **2**, 1214–1222.
27 J. Qiu, Y. Xia, Y. Chen and W. Huang, Management of Crystallization Kinetics for Efficient and Stable Low-Dimensional Ruddlesden-Popper (LDRP) Lead-Free Perovskite Solar Cells, *Adv. Sci.*, 2019, **6**, 1800793.
28 X. Meng, Y. Wang, J. Lin, X. Liu, X. He, J. Barbaud, T. Wu, T. Noda, X. Yang and L. Han, Surface-controlled oriented growth of $FASnI_3$ crystals for efficient lead-free perovskite solar cells, *Joule*, 2020, **4**, 902–912.
29 D. Di Girolamo, J. Pascual, M. H. Aldamasy, Z. Iqbal, G. Li, E. Radicchi, M. Li, S.-H. Turren-Cruz, G. Nasti and A. Dallmann, Solvents for processing stable tin halide perovskites, *ACS Energy Lett.*, 2021, **6**, 959–968.
30 X. Jiang, H. Li, Q. Zhou, Q. Wei, M. Wei, L. Jiang, Z. Wang, Z. Peng, F. Wang and Z. Zang, One-step synthesis of SnI_2·(DMSO)x adducts for high-performance tin perovskite solar cells, *J. Am. Chem. Soc.*, 2021, **143**, 10970–10976.
31 F. Gu, C. Wang, Z. Zhao, G. Zhan, Z. Liu, Z. Bian and C. Huang, Tin (II) acetylacetonate as a new type of tin compensator additive for tin-based perovskite solar cells, *ACS Appl. Mater. Interfaces*, 2021, **13**, 44157–44164.
32 T. Wu, X. Liu, X. He, Y. Wang, X. Meng, T. Noda, X. Yang and L. Han, Efficient and stable tin-based perovskite solar cells by introducing π-conjugated Lewis base, *Sci. Chin. Chem.*, 2020, **63**, 107–115.
33 M. Li, W.-W. Zuo, Y.-G. Yang, M. Aldamasy, Q. Wang, S. H. T. Cruz, S.-L. Feng, M. Saliba, Z.-K. Wang and A. Abate, Tin halide perovskite films made of highly oriented 2D crystals enable more efficient and stable lead-free perovskite solar cells, *ACS Energy Lett.*, 2020, **5**, 1923–1929.
34 E. Jokar, P.-Y. Cheng, C.-Y. Lin, S. Narra, S. Shahbazi and E. W. Diau, Enhanced performance and stability of 3D/2D tin perovskite solar cells fabricated with a sequential solution deposition, *ACS Energy Lett.*, 2021, **6**, 485–492.
35 X. Zheng, C. Wu, S. K. Jha, Z. Li, K. Zhu and S. Priya, Improved phase stability of formamidinium lead triiodide perovskite by strain relaxation, *ACS Energy Lett.*, 2016, **1**, 1014–1020.
36 Y. Chen, Y. Lei, Y. Li, Y. Yu, J. Cai, M. H. Chiu, R. Rao and Y. Gu, Strain engineering and epitaxial stabilization of halide perovskites, *Nature*, 2020, **577**, 209–215.
37 K. Nishimura, D. Hirotani and M. A. Kamarudin, Relationship between Lattice Strain and Efficiency for Sn-Perovskite Solar Cells, *ACS Appl. Mater. Interfaces*, 2019, **11**, 31105–31110.
38 M. I. Saidaminov, J. Kim, A. Jain, R. Y. Zhao, O. Voznyy and E. H. Sargent, Quintero-Bermudez Suppression of atomic vacancies via incorporation of isovalent small ions to increase the stability of halide perovskite solar cells in ambient air, *Nat. Energy*, 2018, **3**, 648–654.
39 D. Gao, B. Li, Z. Li, X. Wu, S. Zhang, D. Zhao, X. Jiang, C. Zhang, Y. Wang, Z. Li, N. Li, S. Xiao, W. C. H. Choy, A. K.-Y. Jen, S. Yang and Z. Zhu, Highly Efficient Flexible Perovskite Solar Cells through Pentylammonium Acetate Modification with Certified Efficiency of 23.35%, *Adv. Mater.*, 2023, **35**, 2206387.
40 T. W. Jones, A. Osherov, M. Alsari and M. Sponseller, Lattice strain causes non-radiative losses in halide perovskites, *Energy Environ. Sci.*, 2019, **12**, 596–606.
41 Z. Huang, X. Hu, C. Liu, L. Tan and Y. Chen, Nucleation and crystallization control via polyurethane to enhance the bendability of perovskite solar cells with excellent device performance, *Adv. Funct. Mater.*, 2017, **27**, 1703061.
42 J. Jiang, Q. Wang, Z. Jin, X. Zhang, J. Lei, H. Bin, Z. G. Zhang, Y. Li and S. F. Liu, Polymer doping for high-efficiency perovskite solar cells with improved moisture stability, *Adv. Energy Mater.*, 2018, **8**, 1701757.
43 W. Feng, C. Zhang, J. X. Zhong, L. Ding and W. Q. Wu, *Chem. Commun.*, 2020, **56**, 5006–5009.
44 X. Zheng, Y. Hou, C. Bao, J. Yin, F. Yuan, Z. Huang, K. Song, J. Liu, J. Troughton, N. Gasparini, C. Zhou, Y. Lin, D.-J. Xue, B. Chen, A. K. Johnston, N. Wei, M. N. Hedhili, M. Wei, A. Y. Alsalloum, P. Maity, B. Turedi, C. Yang, D. Baran, T. D. Anthopoulos, Y. Han, Z.-H. Lu, O. F. Mohammed, F. Gao, E. H. Sargent and O. M. Bakr, *Nat. Energy*, 2020, **5**, 131–140.
45 W. Feng, W. Q. Wu and L. Ding, *J. Energy Chem.*, 2021, **53**, 419–421.
46 S.-H. Lee, S. Jeong, S. Seo, H. Shin, C. Ma and N.-G. Park, Acid Dissociation Constant: A Criterion for Selecting Passivation Agents in Perovskite Solar Cells, *ACS Energy Lett.*, 2021, **6**, 1612–1621.
47 Y. Liao, H. Liu, W. Zhou, D. Yang, Y. Shang, Z. Shi, B. Li, X. Jiang, L. Zhang, L. N. Quan, R. Quintero-Bermudez, B. R. Sutherland, Q. Mi, E. H. Sargent and Z. Ning, Highly Oriented Low-Dimensional Tin Halide Perovskites with Enhanced Stability and Photovoltaic Performance, *J. Am. Chem. Soc.*, 2017, **139**(19), 6693–6699.
48 Y. Zhang, B. Li, L. Fu, Y. Zou, Q. Li and L. Yin, Enhanced optical absorption and efficient cascade electron extraction based on energy band alignment double absorbers perovskite solar cells, *Sol. Energy Mater. Sol. Cells*, 2019, **194**, 168–176.
49 S.-Y. Ju, W. I. Lee and H.-S. Kim, Enhanced Phase Stability of Compressive Strain-Induced Perovskite Crystals, *ACS Appl. Mater. Interfaces*, 2022, **14**, 39996–40004.
50 W. Pan, H. Wu, J. Luo, Z. Deng, C. Ge, C. Chen, X. Jiang, W. Yin, G. Niu, L. Zhu, L. Yin, Y. Zhou, Q. Xie, X. Ke, M. Sui and J. Tang, $Cs_2AgBiBr_6$ single-crystal X-ray detectors with a low detection limit, *Nat. Photonics*, 2017, **11**, 726–732.
51 W. Nie, H. Tsai, R. Asadpour, J. Blancon, A. J. Neukirch, G. Gupta, J. J. Crochet, M. Chhowalla, S. Tretiak, M. A. Alam, H. Wang and A. D. Mohite, High-performance photovoltaic perovskite layers fabricated through intramolecular exchange, *Science*, 2015, **347**, 522–525.
52 A. Rajagopal, P.-W. Liang, C.-C. Chuen, Z. Yang and A. K.-Y. Jen, Defect passivation via a graded fullerene heterojunction in low-bandgap Pb–Sn binary perovskite photovoltaics, *ACS Energy Lett.*, 2017, **2**, 2531–2539.